# Chemical Kinetics of the Interaction of H$_2$O Vapor with Soot in the Range 190 K ≤ *T* ≤ 300 K: A Diffusion Tube Study

## C. Alcala-Jornod[†] and M. J. Rossi*

*Laboratoire de Pollution Atmosphérique et Sol (LPAS), Institut des Sciences et Technologie de l'Environnement (ISTE/ENAC), Ecole Polytechnique Fédérale de Lausanne (EPFL), CH-1015 Lausanne, Switzerland*

*Received: May 20, 2004; In Final Form: August 31, 2004*

The interaction of H$_2$O vapor with flame soot has been investigated in the molecular flow regime with use of the molecular diffusion tube technique over a sizable temperature range. The primary real-time data consist of time-dependent mass spectrometric signals and enable the determination of the initial uptake coefficient $\gamma_0^{MC}$, the surface residence time $\tau_s$ of adsorbed H$_2$O, and the number $n_s$ of adsorption sites per square centimeter of soot substrate surface after applying a Monte Carlo trajectory model that accounts for surface saturation by the H$_2$O pulse propagating across the tube. Typical values at 298 ± 2 K are $\gamma_0^{MC} < 2 \times 10^{-3}$ and $\tau_s < 5$ ms for toluene, acetylene, and diesel soot whereas decane soot does not show any measurable interaction at 298 K. A detailed study of the interaction of H$_2$O with well-characterized decane soot at lower temperature results in the following Arrhenius parameters for desorption of H$_2$O from gray soot generated from a fuel-rich diffusion flame, $\log(1/\tau_s) = (8.8 \pm 0.5) - (7.0 \pm 0.5)/RT$, and from black soot generated in a lean decane diffusion flame, $\log(1/\tau_s) = (8.5 \pm 0.5) - (9.0 \pm 0.6)/RT$ with $R = 1.987 \times 10^{-3}$ kcal/(mol K). These expressions reveal $\tau_s$ of 160 ms at 193 K and 400 ms at 243 K for gray and black decane soot, respectively. Spiking the fuel with thiophene (C$_4$H$_4$S) up to 500 ppm mass fraction (0.05%) does not lead to any change in the H$_2$O adsorption behavior, and saturation experiments with H$_2$O pulses reveal the limited number of H$_2$O adsorption sites on soot accounting for a few percent of the surface carbon atoms. Some atmospheric implications are discussed.

## Introduction

Atmospheric aerosol particles represent the single most uncertain factor in climate change owing to radiative forcing of the recognized contributors such as greenhouse gases and tropospheric aerosols and remain therefore a focal point in atmospheric research.[1,2] Compared to the direct radiative forcing of aerosol particles involving solar and terrestrial radiation in the upper troposphere (UT), the indirect effect of aerosols on cloud formation is still not completely understood today.[1] Of primary concern is the formation of ice clouds in the UT, so-called Cirrus clouds, that is enabled by the presence of small (aerosol) particles that provide the nuclei for ice crystals[3] together with the existence of large ice supersaturated regions in the UT.[4,5] In addition, contrails are visible line-shaped ice clouds that form in the wake of aircraft when the relative humidity in the plume of exhaust gases mixing with the air temporarily reaches liquid saturation so that liquid droplets at first form on cloud condensation nuclei and soon thereafter freeze to ice particles.[6] These conditions have been expressed as the extended Appleman criterion,[7,8] which states that the contrail becomes visible and stable only if the atmospheric H$_2$O partial pressure ($P_{H_2O}$) exceeds the saturation pressure for supercooled liquid water.[9] This empirical relationship suggests the transient formation of a liquid aerosol as a precursor to the ice contrail particles although no pertinent in situ observations have been made. These ice particles may either quickly

evaporate when the ambient air is dry or persist for hours when the air is supersaturated with respect to ice.[5] Statistically significant trends in Cirrus cloudiness over the last two decades have been found at certain latitudes[10,11] and have been attributed to increases in air traffic within the high air traffic corridors of North America, North Atlantic, and Europe.

Aircraft engines emit aerosol particles such as soot and metal particles, gases such as CO, CO$_2$, NO$_x$, and SO$_2$, organic compounds such as hydrocarbons, and condensable gases such as water vapor and sulfuric acid into the UT,[12−14] the latter of which presumably forms liquid particles in the early plume by homogeneous nucleation processes. Aircraft emissions may induce Cirrus cloud formation owing to the presence of sulfuric acid particles and soot.[15] They contribute to the formation of persistent Cirrus clouds far from the emission source after medium to long-range transport giving rise to aviation-induced Cirrus clouds after heterogeneous ice nucleation on insoluble particles of aviation exhaust.[3,16] Black carbon (BC) particles are found to be one of the main constituents of the background aerosol in the UT where climate change owing to radiative imbalance is most dominant.[17−19] Blake and Kato have established a correlation of BC abundance in the UT with air traffic and observations in the near-field of aircraft have confirmed that the insoluble aerosol mode of jet exhaust mainly consists of BC particles.[20,21]

Laboratory-generated soot aerosol shows a surprising manifold of affinities for the interaction with H$_2$O vapor in terms of cloud condensation and ice nucleation abilities, which among other factors depend on both the combustion device and the fuel mixture.[22,23] Like graphite, freshly emitted soot from a combustion device is hydrophobic, that is nonwettable at 298

* To whom correspondence should be addressed. E-mail: michel.rossi@epfl.ch.
† Work performed in partial fulfillment of the requirements for obtaining the degree Dr. ès sc. at EPFL (Thesis No. 2655, 2002).

± 2 K, which leads to large measured contact angles measured for instance with the sessile drop technique.[24-26] Intuitively, the nonwetting properties of BC were taken as an indication of repulsive interaction of soot toward water vapor. It also has led to the hypothesis that the soot interface had to contain adsorbed polar molecules or polar surface functional groups enabling water adsorption to BC. Therefore, the concept of chemical activation of soot through adsorption of water-soluble species such as $H_2SO_4$ was introduced to retain soot as a substance with potential ice nucleating abilities[26,27] despite the fact that no significant quantities of $H_2SO_4$ adsorbed on aviation soot particles have been found in field experiments so far.

In contrast to the statement that soot particles should be activated by $H_2SO_4$ before they are able to adsorb water vapor in order to become hydrophilic,[8,28-31] we show in the present work that flame soot contains sufficient active surface sites for $H_2O$ adsorption without the need of prior adsorption of $H_2SO_4$ in what seems to be a sulfur-free pathway to $H_2O$ adsorption. Field observations on the number density of soot aerosol as a function of contrail age resulted in strong evidence that a significant fraction of soot aerosol, say roughly one-third, yielded ice nuclei without prior adsorption of $H_2SO_4$, which therefore is evidence for a S-free pathway to contrail formation based on soot as the condensation nuclei.[28,32] Similar conclusions have been reached from Cirrus observations as well as from laboratory work.[3,29,30,33-35] Recently, Gorbunov et al. have shown that the ice nucleating ability of soot aerosols is mainly influenced by the particle size and the surface concentration of functional groups that are able to form hydrogen bonds with $H_2O$ molecules. They observed ice particle formation in a cloud chamber by using soot from a diffusion flame and exposed it to an atmosphere supersaturated with respect to ice.[33] We show here that flame soot generated in the laboratory may provide a significant number of sites for $H_2O$ adsorption from 298 ± 2 K down to 193 K without prior activation by $H_2SO_4$.

In the first part of this work that is exploratory in nature we have focused our attention on the interaction of $H_2O$ at 298 ± 2 K with five different types of soot generated from flames of decane, octane, toluene, diesel (commercial sample), and acetylene in air. The second part of the present work lays the groundwork for a molecular understanding of the initial stages of heterogeneous ice nucleation by measuring the adsorption of $H_2O$ molecules on soot from a rich and lean decane diffusion flame in air at low temperatures down to 193 K. The rich decane flame leads to "gray" soot whereas the lean flame forms "black" soot where combustion takes place in a controlled diffusion flame. We show that a significant number of $H_2O$ molecules stay adsorbed on the surface of decane soot during tens to hundreds of milliseconds before desorbing at low temperature. This result may have significant implications for the growth of ice crystals and Cirrus cloud particles given the appropriate temperature and water vapor supersaturation conditions. A preliminary account of parts of the present work has recently been published.[36]

**Experimental Details**

For the study of the interaction of $H_2O$ vapor on flame soot at $T = 298 ± 2$ K, the diffusion tube apparatus described in detail by Koch et al.[37,38] has been used. In the first part of this work we have focused our attention on $H_2O$ interaction with five different types of soot, of which four, namely decane, octane, toluene, and diesel (commercial sample), were generated from the combustion of liquid fuel in a simple burner displayed in panel 1A of Figure 1 that is equipped with a cotton wick
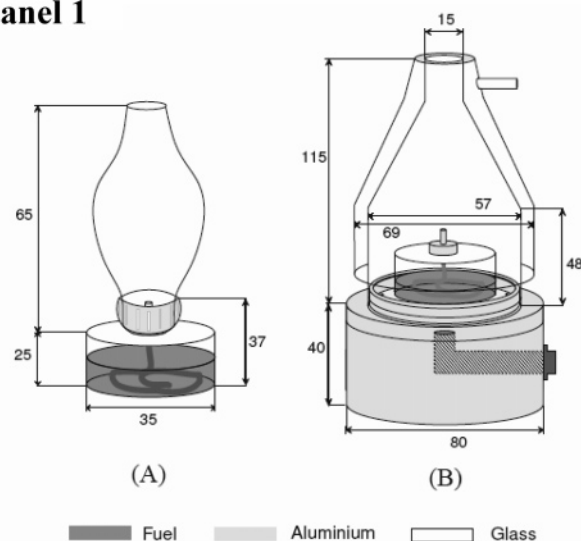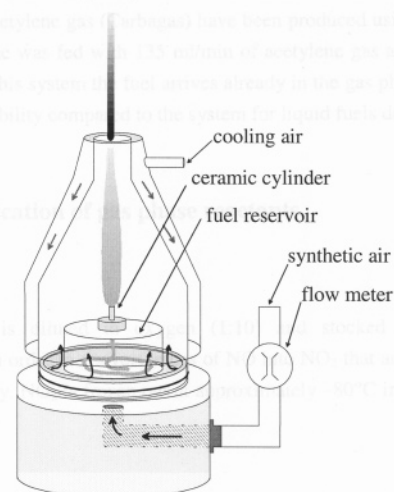


**Figure 1.** Schematic drawing of the burners used to generate soot from liquid fuels. Panels 1A and 1B display the dimensions of the simple burner and co-flow burner, respectively. Panel 2 presents a functional description of the co-flow burner used to generate black and gray decane soot.

extending into the liquid fuel reservoir. Systematic comparison of the physical properties of decane soot generated in the simple burner with soot generated in the co-flow burner displayed in panel 1B and panel 2 of Figure 1 and discussed below[39] reveals that it corresponds to soot originating from a fuel-rich flame, so-called gray soot. In addition, measured values of the surface residence time $\tau_s^m$ discussed below indicate the same. Acetylene has been chosen because of its facile soot production and the possibility to allow for accurate fuel mass flow control and reproducibility in setting of the fuel/air ratio with use of a Bunsen burner.

As briefly pointed out above the first part of this study involved an exploratory study of $H_2O$−soot interaction with soot samples generated in a simple burner displayed in panel 1A of Figure 1. This simple burner supports a diffusion flame equipped with a wick extending into the liquid fuel reservoir without the possibility of adjusting both air and fuel flow. It has been replaced with a co-flow burner displayed in panels 1B and 2 of Figure 1 that has been systematically used with decane fuel to enhance the reproducibility of the kinetic results discussed below. This co-flow burner supports a diffusion flame fed by a flow of compressed air (5% rh) controlled by a mass flow meter

**TABLE 1: Soot Generation Parameters for Decane in the Co-flow Burner Displayed in Panel 1B of Figure 1 and Acetylene Soot in a Bunsen Burner and Elemental Analysis of Decane and Acetylene Soot Obtained in the Co-flow (Panel 1B of Figure 1) and a Bunsen Burner[a]**

| (A) Generation Parameters | | | | | | |
|---|---|---|---|---|---|---|
| flame type | flame height [mm] | flame color | soot deposition [mg min⁻¹] | air flow [L min⁻¹] | fuel duct (pore ∅) [μm] | soot type |
| decane | | | | | | |
| rich | ~60 | orange-red | 2.0 ± 0.5 | 1.2−1.4 | 17−40 | "gray" |
| lean | ~55 | yellow-white | 0.8 ± 0.4 | 1.3−1.5 | 11−16 | "black" |
| acetylene | ~35 | yellow | 1.7 ± 0.5 | | | |

| (B) Elemental Analysis | | | | |
|---|---|---|---|---|
| type of soot | C [% wt] | H [% wt] | N [% wt] | O [% wt] |
| acetylene | 98.26 ± 0.08 | 0.15 ± 0.02 | 0.16 ± 0.08 | 1.41 ± 0.02 |
| "black" decane | 96.39 ± 0.22 | 0.19 ± 0.01 | 0.27 ± 0.09 | 3.22 ± 0.25 |
| "gray" decane | 97.27 ± 0.05 | 0.83 ± 0.04 | 0.2 ± 0.18 | 1.65 ± 0.19 |

[a] The uncertainties correspond to one standard deviation.

(5 L min⁻¹ maximum flow). The glass hood is cooled by ambient air circulating within the double wall, and the fuel is fed by capillary forces across a cotton wick that is topped by a fritted disk made out of Pyrex (3.3 bore) of defined porosity to prevent the combustion of the cotton wick. Two porosities, namely nos. 3 and 4 corresponding to pore diameters of 17−40 and 11−16 μm, respectively, afford the control of the flow of decane into the combustion zone of the diffusion flame. Panels 1A and 1B of Figure 1 present the dimensions of both burners in millimeters.

Two distinctly different kinds of decane soot resulting from a diffusion flame have been generated in the co-flow burner depending on the fuel/air ratio used. One type produced in a fuel-rich flame was called "gray" soot because of its gray tinge. The second type was obtained in a lean flame and was called "black" because of its pitch black appearance. The rich flame is characterized by an orange-red emission, is slightly diffuse, and produces a soot plume 5−6 mm wide. The lean flame resulting in black soot has a more intense emission characterized by a white-yellow flame and generates a thinner soot plume 2−3 mm wide. Characteristic data in relation to the production of gray and black decane soot are displayed in Table 1A. No quantitative fuel-to-oxygen ratios of diffusion flames leading to black and gray flame soot have been measured in this work in contrast to work performed on hexane and octane soot with the CAST (Combustion Aerosol STandard) burner[40,41] that resulted in the corresponding black and gray soot, respectively. Acetylene soot has been obtained with use of a Bunsen burner whose air duct was plugged to enhance the rate of soot production. The flow of C₂H₂ gas was regulated with a mass flow controller (1 L min⁻¹ maximum flow) whose flow was commonly set to 67.5 cm³ min⁻¹, giving rise to a yellow flame 4 cm high (Table 1A).

Black and gray decane as well as acetylene soot obtained in the way described above have been characterized by numerous methods.[39,41] The elemental analysis is presented in Table 1B, which suggests that acetylene soot has a similar composition to gray decane soot whose BET surface area measured with N₂ at 77 K is 218 compared to 69 m² g⁻¹ for black soot.[39] The diameter of the primary soot particles of gray soot is 40 nm as opposed to 20 nm for black soot.[40] Owing to the more important fraction of organic material adsorbed on gray compared to black soot, close-up TEM images of gray soot present a "sticky" appearance involving larger primary combustion particles that are aggregated to particles compared to black soot that is "drier" in appearance. Additional data including electronic microscopy (SEM, TEM), electron diffraction, the analysis of burnt gases

(residual MS), the combustion aerosol particle size distribution (DMA-CNC), and the analysis of the amount of adsorbed sulfate (IC) and total adsorbed sulfur (ICP) on both gray and black decane soot may be found in the PhD thesis of Alcala-Jornod.[42]

Soot samples have been generated by directly flowing the burnt gases of a diffusion flame through the diffusion tube. The diffusion tube experiment consists of injecting a known quantity of H₂O vapor on the order of 10¹⁴ to 10¹⁵ H₂O molecules into a tube coated with soot and recording the arrival time of H₂O monitored by time-dependent residual gas mass spectrometry (MS) at $m/e$ 18 under molecular flow conditions after the admission of the water vapor pulse. This experiment (sample) is compared to the noninteracting case (reference) where an identical H₂O pulse is propagating across a FEP (Fluorinated Ethylene Propylene copolymer)-coated tube of the same dimension as the sample tube. This technique enables the measurement of the real-time kinetics of molecular desorption when an appropriate assumption regarding the mass accommodation coefficient is made. A simulation model with Monte Carlo trajectories is used to fit the experimental time-dependent MS trace. The model has been described in detail before [38,43] and is used when the experimental signals show a complex, that is nonexponential decay owing to saturation of the soot surface that varies along the tube axis. The numerical simulations succeed in modeling the experimental signals over a range of experimental conditions with only three fitting parameters, namely $\tau_s$, the surface residence time of H₂O adsorbed on the soot substrate, the initial uptake coefficient $\gamma_0^{MC}$ leading to irreversible removal of H₂O vapor, and $n_s$, the number of active surface sites for the heterogeneous H₂O−soot interaction. Experiments have been performed at ambient temperature of 25 ± 2 °C (298 ± 2 K).

The temperature-dependent diffusion tube experiments have been performed exclusively on decane soot and consist of injecting a known quantity of H₂O vapor into a tube coated with soot that is maintained at the desired low temperature thanks to the circulation of cold methanol (at −80 °C) or ethylene glycol (down to −30 °C). The temperature control in both cases is to within 0.5 K. The same Monte Carlo simulation model with the three parameters mentioned above is used to fit the experimental time-dependent MS trace. Experiments have been performed from ambient temperature at 25 ± 2 °C down to −80 °C (193 K) and −30 °C (243 K) for gray and black soot, respectively.

Two aspects of the interaction of H₂O with soot have been emphasized in this work: The reaction mechanism as well as the kinetics of the heterogeneous interaction. The uptake

coefficient $\gamma_0$ or reaction probability, defined as the fractional probability per collision for the disappearance of $H_2O$ from the gas phase on the time scale of the experiment, may be determined by measuring the mass balance ratio of the surviving fraction relative to the total number of injected molecules. However, because most soot samples showed saturation by $H_2O$ vapor the resulting MS arrival time curves showed a complex decay such that we had to resort to the Monte Carlo trajectory model to simulate the experimental MS signal and to determine the resulting kinetic parameters $n_s$, $\tau_s$, and $\gamma_0^{MC}$ by curve fitting to the raw MS signals [43] that is not to be confused with the measured quantities $\gamma^m$ and $\tau_s^m$.

## Results and Discussion

**Interaction of $H_2O$ with Different Samples of Flame Soot at $298 \pm 2$ K (Ambient Temperature).** In an exploratory phase of our work experiments have been performed on $H_2O$ vapor interacting with five types of soot generated from a diffusion flame of decane, octane, toluene, acetylene, and diesel fuel in air using the simple burner displayed in panel 1A of Figure 1 to see whether there is a measurable $H_2O$/soot interaction. Uptake experiments of $H_2O$ in a Knudsen flow reactor at $298 \pm 2$ K did not result in any measurable interaction, presumably because the surface-to-volume ratio ($S/V$) of the flow reactor is significantly smaller than that for the diffusion tube: a typical value for a flow reactor is $S/V = 0.01$ vs 2.0 for the diffusion tube. The arrival time $t_{arr}$ is defined as the inverse of the decay constant $k$ of the time-dependent MS signal. It is determined by fitting the decaying portion of the MS signal ($I(t)$) to a single-exponential decay according to eq 1:

$$I(t) = I_0 \exp(-kt) \text{ with } 1/k = t_{arr} \qquad (1)$$

Under the normal operating conditions of molecular flow within the diffusion tube the collision number $Z$ is given solely by the geometry of the tube and is calculated by using the Monte Carlo numerical model for the different tubes used in the present work. For an interactive but nonreactive system such as the present one the surface residence time of the average molecule $\tau_s^m$ may be calculated directly by comparing the arrival time of the interactive gas/surface system ($1/k$) to that of the noninteracting (reference, FEP-coated tube) case given by $1/k_{ref}$ according to eq 2:

$$\tau_s^m = ((1/k) - (1/k_{ref}))/Z \qquad (2)$$

This expression is based on the assumption that the arrival time in the interactive case ($1/k$) is the sum of the gas phase ($\tau_g$) and surface ($\tau_s$) residence times, whereas the arrival time for the noninteractive reference case equals $\tau_g$ only. We thus have $1/k + 1/k_{ref} = Z\tau = Z(\tau_g + \tau_s)$ that is equivalent to eq 2. This simple analysis breaks down in interactive cases that include chemical reaction and/or surface saturation processes in which case Monte Carlo trajectories have to be fitted to the experimental arrival time curves. Nevertheless, even in the present case where partial surface saturation during a pulse takes place the measured values of $\tau_s^m$ and $\gamma^m$, the measured surface residence time and uptake coefficient, characterize the experimental data and are therefore listed in Tables 2−4 even though they are not directly related to elementary processes of the $H_2O$/soot system. The uptake coefficient $\gamma^m$ is based on the number of surviving molecules effusing out of the diffusion tube and is determined by using a calibration plot that has been obtained with the Monte Carlo trajectories for a given tube geometry according to a procedure described in the literature.[38,43,44]
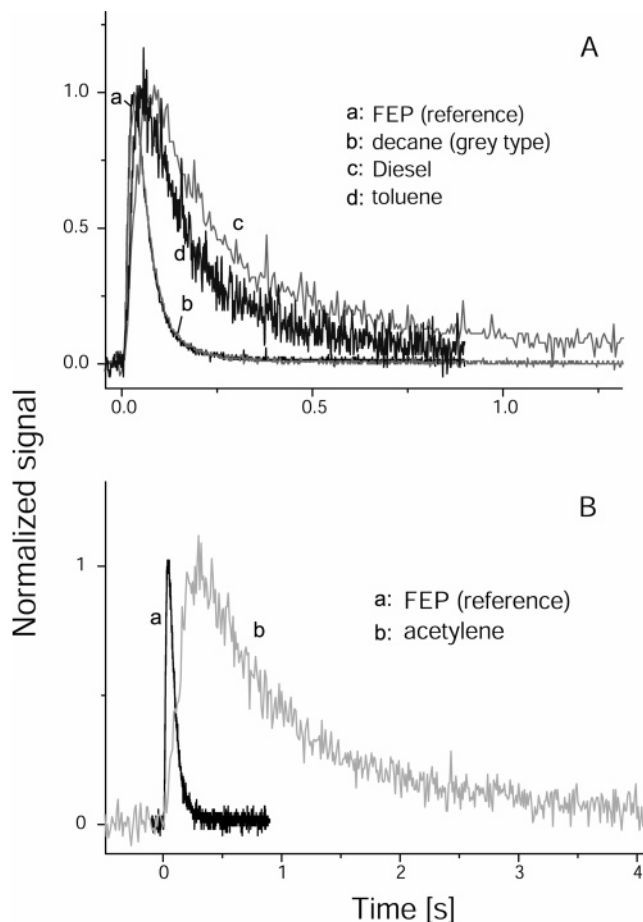


**Figure 2.** Scaled experimental arrival time of $H_2O$ monitored at $m/e$ 18 interacting on FEP (reference), toluene, decane (gray soot), and diesel soot performed in a $2 \times 35$ cm$^2$ tube ($Z = 535$) (panel A) and on FEP and acetylene soot performed in a $2 \times 50$ cm$^2$ ($Z = 1150$) tube (panel B). The injected doses range from $6 \times 10^{14}$ to $6.9 \times 10^{14}$ $H_2O$ molecules at $298 \pm 2$K.

However, in the present case of simultaneous saturation and possible reactive disappearance both $\gamma^m$ and $\tau_s^m$ cannot be determined separately and a numerical model must be used.

As an example, Figure 2 displays the interactive and reference, that is the noninteractive MS signal for $H_2O$ vapor interacting with FEP−Teflon (reference), diesel, toluene, and decane (gray) in panel A and acetylene soot in panel B. The amplitudes have been scaled to emphasize the different shapes of the temporal decay. Water vapor definitely has a measurable surface residence time $\tau_s$ owing to the increase in the arrival time of $H_2O$ for the interactive cases compared to the reference case. However, very few or no $H_2O$ molecules are lost on the soot substrate on the time scale of the experiment as a result of this interaction because the integrals of the interactive and reference MS signals are equal or very similar to each other, thus indicating a nonreactive albeit interactive situation leading to reversible uptake of $H_2O$ on soot. Table 2 summarizes the results for $H_2O$ interacting with the different types of soot with use of the simple Monte Carlo model described in detail by Alcala-Jornod and Rossi.[43] The quality of the Monte Carlo fit is excellent for all four tested soot substrates as may be seen in Figure 3 for the example of the interaction of $H_2O$ on diesel soot, which clearly shows the nonexponential behavior of the decaying MS signal and therefore provides ample justification for the application of the Monte Carlo model to the MS data resulting in the fitting parameters $n_s$, $\tau_s$, and $\gamma_0^{MC}$. These parameters are compared in Table 2 to the measured values $\gamma^m$

Interaction of H$_2$O Vapor with Soot

*J. Phys. Chem. A, Vol. 108, No. 48, 2004* **10671**

**TABLE 2: Kinetic Parameters for the Reaction of H$_2$O on Toluene, Acetylene, Decane, Octane, and Diesel Soot[a] at 298 ± 2K**

| soot | tube [cm$^2$] | dose[b]/10$^{14}$ [molecule] | 10$^{-2}\gamma^m$ | $\tau_s^m$ [ms] | fitting parameters 10$^{12}n_s$ [cm$^{-2}$] | 10$^{-2}\gamma_0^{MC}$ | $\tau_s$ [ms] |
|---|---|---|---|---|---|---|---|
| toluene | 2 × 35 | 6 | 0.2 | 0.2−1.5 | 2.5 | 0.2 | 2 |
| | 2 × 35 | 8 | | 0.7 | | | |
| acetylene | 2 × 50 | 6.5 | 0 | 0.86 | 3 | 0 | 2.5 |
| | 2 × 50 | 7.3 | 0.017 | 1.9 | 4 | 0.017 | 5 |
| | 2 × 50 | 7.2 | 0 | 0.3−1.4 | | | |
| | 2 × 50 | 7.3 | | 1.7 | | | |
| decane | 2 × 35 | 6.9 | 0 | 0.01 | 1.7 | 0.1 | 0.2 |
| | 2 × 25 | 1.3 | 0 | 0.02 | 0.5 | 0 | 0.2 |
| octane | 2 × 35 | 6.9 | 0 | 0.04 | | | |
| | 2 × 35 | 3 | 0.03 | 0.02−0.04 | | | |
| diesel | 2 × 35 | 7 | | 0.2 | 3.1−3.2 | 0−0.05 | 4−6 |
| | 2 × 35 | 6.9 | 0 | 0.1 | 3.2 | 0 | 3 |
| | 2 × 30 | 0.83 | 0 | 0.3−0.4 | | | |
| | 2 × 30 | 4.5 | 0 | 0.4 | | | |

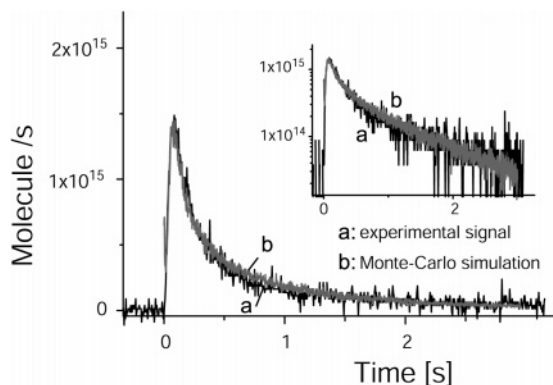[a] Every entry corresponds to a new sample. [b] Uncertainty in the dose is 10−20%.



**Figure 3.** Experimental arrival time of H$_2$O monitored at *m/e* 18 interacting with diesel soot at 298 ± 2 K performed in a 2 × 35 cm$^2$ tube ($Z$ = 535) and the corresponding Monte Carlo fit with use of the one site model with the following fitting parameters: $n_s$ = 3.2 × 10$^{12}$ cm$^{-2}$, $\gamma_0^{MC}$ = 0, $\tau_s$ = 3 ms, and a dose of 6.9 × 10$^{14}$ molecules.

and $\tau_s^m$ discussed above, where the latter value has been obtained from the initial fast decaying portion of the arrival time curve as displayed in the logarithmic portion of Figure 3.

The main result averaged over all soot samples except decane is an uptake coefficient $\gamma_0^{MC}$ that is lower than 2 × 10$^{-3}$, and surface residence times $\tau_s$ between a fraction and a few milliseconds. Moreover, we note that the number of surface sites $n_s$ is approximately the same for the four considered fuels toluene, acetylene, decane, and diesel at comparable doses with a maximum interval between the lowest and the highest value of a factor of 2. However, akin to the interaction of NO$_2$ with soot[43] we observe a dependence of $n_s$ with the dose where higher doses of H$_2$O require a higher value of $n_s$. We also may point out the good agreement between $\gamma^m$ displayed in the fourth column of Table 2 and its fitted value $\gamma_0^{MC}$ presented in column seven of Table 2 that is undoubtedly a consequence of its small value, which apparently leads to separability between irreversible ($\gamma_0^{MC}$) and reversible ($\tau_s$) H$_2$O adsorption. However, the discrepancy between $\tau_s^m$ and $\tau_s$ amounts to a factor of 10 or so that is due primarily to saturation processes that are not taken into account in $\tau_s^m$. H$_2$O molecules within the same pulse that collide with an already occupied adsorption site do not contribute to the residence time of the average molecule and exit the diffusion tube earlier than an average molecule interacting with a less saturated substrate. This disagreement between $\tau_s^m$ and $\tau_s$ reveals once more the importance of taking into account
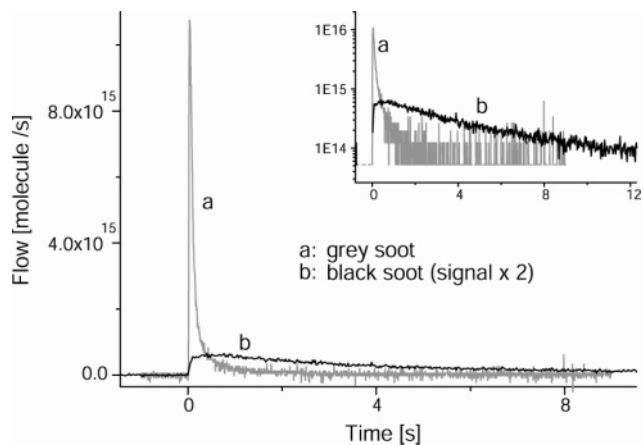


**Figure 4.** Experimental arrival time of H$_2$O monitored at *m/e* 18 interacting with black and gray decane soot performed in a 1.1 × 29.5 cm$^2$ tube ($Z$ = 1190) at 25 ± 2 °C. The dose is 1.7 × 10$^{15}$ and 2.2 × 10$^{15}$ of injected H$_2$O molecules for experiments with gray and black decane soot, respectively.

saturation processes that occur on the surface of the soot sample in our Monte Carlo trajectory. Finally, we may see that $\tau_s$ for decane soot is smaller by a factor 10−25 compared to the other types of soot. This is apparent in Figure 2A where the arrival time curve of decane is not significantly different from the reference and indicates the unusually low value of $\tau_s$ for H$_2$O adsorbed on decane soot, presumably because of the presence of the adsorbed organic phase that blocks adsorption sites for H$_2$O vapor. In contrast, black decane soot, which is produced in a diffusion flame richer in oxygen and discussed below, has a value of $\tau_s$ similar to that of toluene, acetylene, and diesel soot at 298 ± 2 K. This result therefore underlines the importance of controlling the combustion conditions within the flame as it determines to a large extent the reactivity of soot toward H$_2$O vapor.

**Interaction of H$_2$O with Black and Gray Decane Flame Soot in the Range 193 K to 298 ± 2 K (Ambient Temperature).** This section deals with a detailed study of the kinetics of H$_2$O vapor adsorption as a function of temperature on decane soot whose flame conditions have been tightly controlled by using the co-flow burner and whose reproducibility has been experimentally verified. The first observation is that H$_2$O shows a measurable interaction with soot already at 298 ± 2 K as may be seen in Figure 4, which displays a comparison between experiments of H$_2$O interacting with gray and black soot. This is in agreement with experiments on H$_2$O interacting with four different types of soot at 298 ± 2 K described above (Table 2). However, an important quantitative difference in the interaction of H$_2$O with the two types of substrates, namely gray versus black soot, has been detected. In fact, black soot shows a much stronger interaction with H$_2$O compared to gray soot already at 298 ± 2 K because of the longer arrival time of signal b (black soot) compared to signal a (gray soot) as displayed in Figure 4. The overall mechanism of the reaction is described in eq 3 where $k_a$ and $k_d$ are the first-order rate constants for adsorption and desorption of H$_2$O on soot, respectively. The surface residence time of adsorbed H$_2$O is expressed as

$$H_2O(g) \underset{k_d}{\overset{k_a}{\rightleftharpoons}} H_2O(ads) \qquad (3)$$
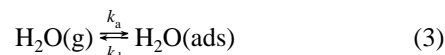
$\tau_s = 1/k_d$, which ranges from a fraction of a millisecond for gray soot to 15 ms on average for black soot at 298 ± 2 K as displayed in Tables 3 and 4 for gray and black soot, respectively.

**TABLE 3: Kinetic Parameters for the Reaction of $H_2O$ on Gray Decane Soot Performed in a $1.1 \times 29.5$ cm$^2$ Tube ($Z = 1190$) at $298 \pm 2$ K and Low Temperature[a]**

| dose[b]/$10^{14}$ [molecule] | $\Phi_{H_2O}$ [%][c] | $10^{-2}\gamma^m$ | $\tau_s^m$ [ms] | $10^{12}n_s$ [cm$^{-2}$] | $10^{-2}\gamma_0^{MC}$ | $\tau_s$ [ms] |
|---|---|---|---|---|---|---|
|  $T = 25 \pm 2$ °C ($298 \pm 2$ K)  | | | | | | |
| 20 | 91 | 0.008 | 0.03 | | | |
| 20 | 123 | 0 | 0.07 | | | |
| 6 | 104 | 0 | 0.02 | | | |
| 18 | n.m. | | | 10 | 0.05 | 0.5 |
| 22 | n.m. | | | 8−12 | 0.02 | 0.1−0.3 |
| 21 | n.m. | | | 12 | 0 | 0.2 |
| 19 | n.m. | | | 12 | 0 | 0.1 |
| 19 | n.m. | | | 14 | 0 | 0.1 |
| 17 | n.m. | | | 11 | 0.05 | 0.5 |
|  $T = -30$ °C (243 K)  | | | | | | |
| 18 | 83 | 0.015 | 0.06 | 14 | 0.1 | 1 |
| 22 | 76−85 | 0.013−0.02 | 0.04 | 12 | 0.06 | 0.4 |
| 22 | 85 | 0.013 | 0.03 | 15 | 0.1 | 0.5 |
| 21 | 66−82 | 0.016−0.04 | 0.3 | 19.5 | 0.2 | 5 |
| 19 | 85 | 0.013 | 0.13 | 16 | 0.15 | 3 |
| 19 | 75−94 | 0.005−0.026 | 0.17 | 16 | 0.15 | 3 |
| 17 | 86 | 0.012 | 0.2 | 15 | 0.1 | 4 |
|  $T = -80$ °C (193 K)  | | | | | | |
| 21 | 51 | 0.071 | 12 | 23 | 0.2 | 100 |
| 19 | 61 | 0.05 | 8 | 19 | 0.15 | 200 |
| 19 | 71 | 0.033 | 9.2 | 22 | 0.05 | 50 |
| 17 | 40 | 0.1 | 25 | 17.5 | 0.1 | 300 |

[a] Every entry corresponds to a new sample. [b] Uncertainty in the dose is 10−20%. [c] Yield of $H_2O$ expressed in percent of injected $H_2O$ molecules.

**TABLE 4: Kinetic Parameters for the Reaction of $H_2O$ on Black Decane Soot Performed in a $1.1 \times 20$ cm$^2$ Tube ($Z = 565$) at $298 \pm 2$ K and Low Temperature[a]**

| dose[b]/$10^{14}$ [molecule] | $\Phi_{H_2O}$ [%][c] | $10^{-2}\gamma^m$ | $\tau_s^m$ [ms] | $10^{12}n_s$ [cm$^{-2}$] | $10^{-2}\gamma_0^{MC}$ | $\tau_s$ [ms] |
|---|---|---|---|---|---|---|
|  $T = 25$ °C (298 K)  | | | | | | |
| 23 | n.m. | | 3−6 | 35 | 0 | 15 |
| 11 | 95 | ~0 | 3−4 | 19 | 0 | 10 |
| 16 | 120 | 0 | 5−7 | 27 | 0 | 20 |
| 21 | n.m. | | 3 | 40 | 0 | 10 |
| 110 | n.m. | | 1 | 150 | 0 | 5 |
|  $T = -10$ °C (263 K)  | | | | | | |
| 22 | n.m. | | ~25 | 39 | 0 | 100 |
| 21 | n.m. | | 20−22 | 35 | 0 | 100 |
| 11 | n.m. | | 30−32 | 18 | 0 | 100 |
| 16 | n.m. | | 28−30 | 27 | 0 | 200 |
|  $T = -30$ °C (243 K)  | | | | | | |
| 23 | n.m. | | ~155 | 40 | 0 | 400 |
| 21 | n.m. | | ~78 | 30 | 0 | 300 |
| 16 | n.m. | | 150 | 27 | 0 | 500 |
| 17 | 83−94 | 0.01−0.03 | | | | |
| 110 | n.m. | | 77 | 180 | 0 | 300 |

[a] Every entry corresponds to a new sample. [b] The uncertainty in the dose is 10−20%. [c] Yield of $H_2O$ expressed in percent of injected $H_2O$ molecules.

As briefly pointed out above a comparison of the values for $\tau_s$ of Tables 2, 3, and 4 confirms that soot generated in the simple burner resembles gray soot whose results are displayed in Table 3. Sample results for raw $H_2O$ time-dependent MS signals at lower temperature are shown in Figure 4, which displays an example of the interaction of $H_2O$ with gray (upper panel) and black (lower panel) decane soot at temperatures down to −80 (193 K) and − 30 °C (243 K) for gray and black soot, respectively.

As expected, the strength of the interaction between both types of soot and $H_2O$ vapor increases as the temperature decreases because $k_a$ is only weakly dependent on temperature and $k_d$ decreases with decreasing temperature owing to the endothermicity of $H_2O$ desorption, eq 3. Surface residence times $\tau_s$, which are summarized in Tables 3 and 4 for gray and black soot, respectively, can reach on average 500 ms at 243 K for black soot, which is the longest residence time measured in the present study. In column 2 of Tables 3 and 4 the yield of effusing $H_2O$ is expressed in percent of injected $H_2O$ molecules. This measurement has been performed by comparing the integrals of the MS signals at low temperature with the ones at $298 \pm 2$ K where the yield was considered as 100% despite the small scatter in the integrals observed among the different experiments at $T = 298$ K. At $298 \pm 2$ K the yield of effusing $H_2O$ molecules on soot has been determined by comparison with reference experiments of $H_2O$/FEP-Teflon. The scatter in the yields obtained at $T = 25$ °C is mainly due to the use of two different pulsed valves, one placed on top of the reference tube and the other on the sample, that is the soot-coated tube. To enable the comparison of the doses dispensed by the two different pulsed valves we had to introduce a scaling factor for matching purposes that also varied with the opening time of each valve. We therefore attribute an uncertainty in the dose on the order of 10−20%, which can lead to yields exceeding 100% as displayed in Tables 3 and 4. Alternatively, uncertainties in the yields may also stem from the integration of MS signals over too short a time period that would undercount some late arriving molecules.

The yields of effusing $H_2O$ that have not been measured are labeled as "n.m." (not measured) in Tables 3 and 4. The yield of surviving $H_2O$ molecules in the case of the $H_2O$/black soot interaction at low temperature has not been measured in most of the experiments because at the end of the observation period the signals did not reach the baseline on the experimental time scale that was limited to a maximum of 90 s for instrumental reasons. However, a few experiments have been performed at $T = -30$ °C on a longer time scale of 6 to 10 min and showed a yield of ~100%, which therefore leads to a value of $\gamma_0 = 0$ as all $H_2O$ molecules are recovered on this time scale. This is also in agreement with the Monte Carlo simulations which successfully fit the time-dependent MS signals with use of $\gamma_0 = 0$ for cases where the $H_2O$ yield is 100% within the experimental uncertainty (Table 4, $T = 25$ °C). Column 3 of Tables 3 and 4 displays the experimental values $\gamma^m$ calculated from the yield expressed in column 2 and the Monte Carlo simulated yield curves that give the yield of surviving molecules as a function of a chosen value of $\gamma_0$ for different tube geometries.[38,44] In conclusion, it seems that $\gamma^m$ is small but nonzero, on the order of $10^{-4}$ to $10^{-3}$ for gray soot (Table 3), whereas $\gamma^m$ seems to be $<10^{-4}$ for black soot (Table 4). We speculate that the adsorbed organic phase present on gray decane soot may include hydrophilic partially oxygenated complex organic hydrocarbons that to a certain extent irreversibly interact with $H_2O$ vapor, whereas such a specific interaction would be largely absent in the case of black soot. This may explain the nonzero value for $\gamma^m$ or $\gamma_0^{MC}$ for gray decane soot despite the blocking of adsorption sites by the abundant organic phase.

Columns 4 of Tables 3 and 4 display the surface residence time $\tau_s^m$ obtained by choosing the initial slope $k_{ini}$ of the logarithmic plot of the arrival time curve and then using eq 2 for the evaluation of $\tau_s^m$. The time-dependent MS signal does not obey a single-exponential decay rate so that we decided to take the initial, that is largest, slope because of the concave
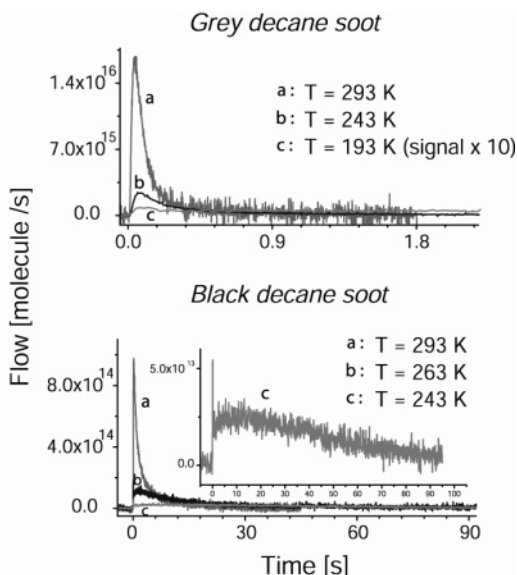
**Figure 5.** Experimental arrival time of $H_2O$ monitored at $m/e$ 18 interacting with gray (upper panel) and black (lower panel) decane soot from $25 \pm 2$ °C ($298 \pm 2$ K) down to $-80$ °C (193 K) and $-30$ °C (243 K) for gray and black soot, respectively. Experiments have been performed in a $1.1 \times 29.5$ cm² ($Z = 1190$) and $1.1 \times 20$ cm² ($Z = 565$) tube at doses of $2.1 \times 10^{15}$ and $2.3 \times 10^{15}$ of injected $H_2O$ molecules for gray and black decane soot, respectively.

shape of the logarithmic plot that always leads to the maximum value in the beginning. We may recall that the experimental values $\gamma^m$ and $\tau_s^m$ have been derived by ignoring saturation processes and therefore do not represent the true kinetic values of the measured interaction but constitute a way to characterize and compare raw experimental signals. The last three columns of both Tables 3 and 4 display the fitting parameters of the Monte Carlo simulations of the MS signals, namely $n_s$, $\tau_s$, and $\gamma_0^{MC}$. These values take into account saturation of adsorption sites on soot, which occurs during the pulse of injected $H_2O$ molecules. The Monte Carlo trajectory model described by Alcala-Jornod and Rossi[43] has been successfully used when the experimental signals show a nonexponential decay owing to a spatially nonhomogeneous saturation of the soot surface along the tube axis that decreases toward the exit of the tube at the detector end.

In contrast to the results for the soot samples examined at $298 \pm 2$ K and displayed in Table 2 the interaction of gray decane soot with $H_2O$ vapor seems to be governed by $\gamma^m < \gamma_0^{MC}$ amounting to roughly a factor of 10 as may be seen in Table 3. Therefore, the uptake coefficient $\gamma^m$ seems to be small but nonzero. For the same reason, $\tau_s^m$ seems to be smaller than $\tau_s$ owing to the occurrence of saturation of adsorption sites on the gray soot substrate. The interaction of water vapor on black decane soot seems to be characterized by an uptake coefficient that is very small or zero as displayed in Table 4. Similar to $\gamma$ for gray decane soot, $\tau_s^m < \tau_s$ by a factor of 3 to 5, again owing to saturation of water adsorption sites on the soot substrate. In addition, a cross comparison of $\tau_s$ between black and gray decane soot reveals the absolute value for the former to be larger by roughly 2 orders of magnitude. Black decane soot therefore interacts more strongly with $H_2O$ vapor than gray soot under identical experimental conditions, presumably because the adsorbed organic phase blocks surface adsorption sites for $H_2O$ vapor.

The good agreement between experimental signals and Monte Carlo simulations with use of the simple one-site model may be seen, for example, in Figure 6, which displays experimental
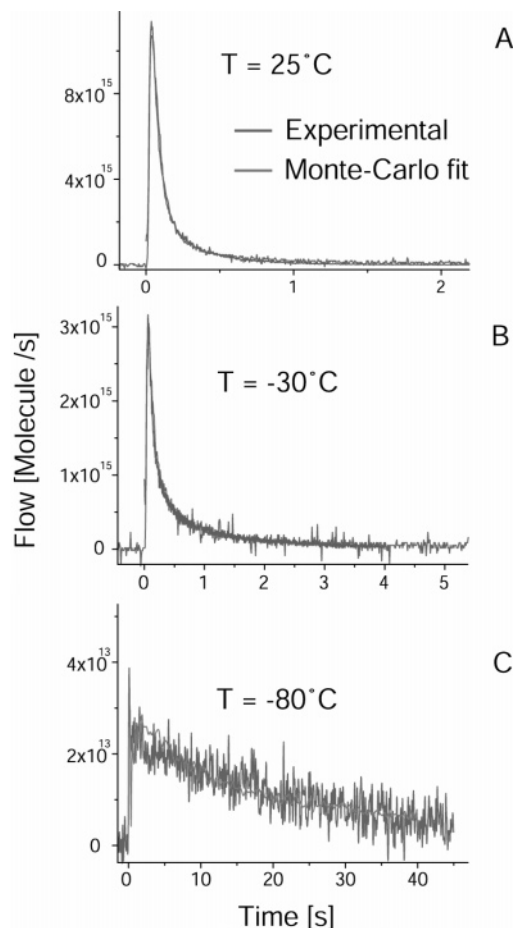


**Figure 6.** Experimental arrival time of $H_2O$ monitored at $m/e$ 18 interacting with gray decane soot from $25 \pm 2$ K ($298 \pm 2$ K) down to $-80$ °C (193 K) performed in a $1.1 \times 29.5$ cm² ($Z = 1190$) tube at a dose of $1.7 \times 10^{15}$ molecules and the corresponding Monte Carlo fits. The fitting parameters are the following: for panel A, $\tau_s = 0.5$ ms, $\gamma_0^{MC} = 0.05 \times 10^{-2}$, $n_s = 11 \times 10^{12}$ cm⁻²; for panel B, $\tau_s = 4$ ms, $\gamma_0^{MC} = 0.1 \times 10^{-2}$, $n_s = 15 \times 10^{12}$ cm⁻²; and for panel C, $\tau_s = 300$ ms, $\gamma_0^{MC} = 0.1 \times 10^{-2}$, and $n_s = 17.5 \times 10^{12}$ cm⁻².

signals of $H_2O$ on gray soot at three different temperatures and their corresponding Monte Carlo fits. Column 5 of Tables 3 and 4 shows the number of active surface sites $n_s$ for adsorption, which is approximately twice as high for black compared to gray decane soot. When we consider a commercially available pure amorphous carbon substrate with densities between 1.8 and 2.1 g/cm³ as is characteristic for "Pigment Blacks" (DEGUSSA) we may calculate a surface density of approximately $2 \times 10^{15}$ C atoms per cm². In that case, only 1 site in 100 would represent an adsorption site for $H_2O$ in our experiments for the case of low-dose experiments. However, if values more typical of the adsorption of polyatomic molecules on soot on the order of $5 \times 10^{14}$ molecules cm² are used, the nominal coverage increases accordingly by a factor of 4. Therefore, we postulate that $H_2O$ adsorption occurs either on surface defects or on impurities of soot or surface functional groups, most probably containing oxygen, which can form hydrogen bonds with water molecules.[29,30,45,46] Moreover, it is interesting to point out that black decane soot, which offers more adsorption sites for $H_2O$, is also the soot whose oxygen content is the highest. Elemental analysis detailed by Stadler and Rossi[39] and displayed in Table 1B shows an oxygen content higher by approximately a factor of 2 for black compared to gray decane soot, that is 3.22 and 1.65 [% wt] for bulk black and gray decane soot, respectively.
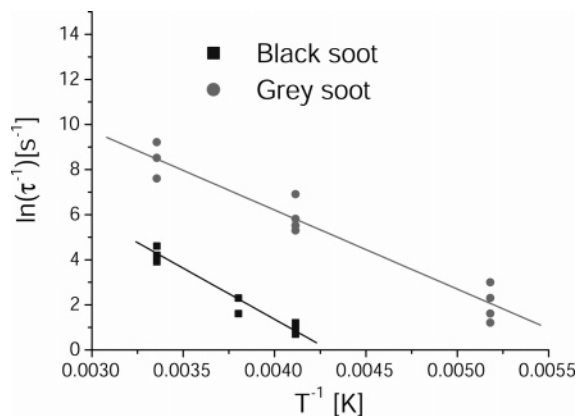
**10674** *J. Phys. Chem. A, Vol. 108, No. 48, 2004*

Alcala-Jornod and Rossi



**Figure 7.** Arrhenius plots of the rate constant of desorption $k_d$ expressed as $k_d = 1/\tau_s = A_d \exp(-E_d/RT)$, using the Monte Carlo fitting parameter $\tau_s$ for the interaction of $H_2O$ on gray and black decane soot. The activation energy for water desorption $E_d = 7.0 \pm 0.5$ and $9.0 \pm 0.6$ kcal/mol for gray and black soot, respectively, whereas the preexponential factor $\log A_d/s^{-1} = 8.8 \pm 0.5$ (gray soot) and $8.5 \pm 0.5$ (black soot).

The activation parameters, namely the activation energy $E_d$ and the preexponential $A$ factor for desorption of water from the soot substrate, have been calculated for both gray and black decane soot from the temperature dependence of its rate constant $k_d$. It is equivalent to the enthalpy of desorption of $H_2O$ from the soot substrate in the absence of an activation energy for $H_2O$ adsorption, which is usually assumed to be the case barring any negative activation energy for adsorption which has been observed on occasion.[47,48] The result is $E_d = 7.0 \pm 0.5$ and $9.0 \pm 0.6$ kcal/mol for gray and black soot, respectively. The Arrhenius representation of the rate constant for desorption, $k_d$, expressed as $k_d = A_d \exp[-E_d/RT]$ has also been determined. The values of $\log A_d$ ($s^{-1}$) are $8.8 \pm 0.5$ and $8.5 \pm 0.5$ for gray and black soot, respectively. Figure 7 displays the two Arrhenius plots for black and gray decane soot, using the Monte Carlo fitting parameter $\tau_s$ leading to $k_d = 1/\tau_s$ based on the values of Table 5 that presents a summary of the kinetic parameters.

Compared to the enthalpy of sublimation of 12.2 kcal/mol for $H_2O$ from bulk ice[49] we find a value for the desorption of $H_2O$ from the two types of soot that is significantly smaller. The water partial pressure during a pulse of $H_2O$ is not high enough to maintain supersaturation conditions for ice formation. We have calculated that the partial pressure of $H_2O$ in the tube reaches the saturation value of ice when all the injected molecules are distributed within the first 5 cm of a $1.1 \times 29.5$ cm$^2$ tube at $T = 193$ K, which are the most favorable conditions for supersaturation. A Monte Carlo simulation shows that after 0.1 ms 97% of the injected molecules are confined within the first 5 cm of a $1.1 \times 29.5$ cm$^2$ tube. Table 6 displays quantitative data.

This means that in the first 0.1 ms following the injection of $H_2O$ molecules supersaturation conditions are maintained, which is insignificant in regards to the time scale of several minutes during which $H_2O$ vapor interacts with gray soot at 193 K after admitting a $H_2O$ pulse. Therefore, we do not expect to observe the growth of water droplets or ice particles on the soot surface using our technique as only the first step of wetting the soot surface with water is studied in our experiment. This wetting or activation process may be thought of as laying the groundwork for additional condensation of $H_2O$ vapor given the appropriate super saturation conditions which may ultimately lead to the nucleation of atmospheric ice aerosols. Nevertheless, water nucleation on black decane soot leading to droplets several

micrometers in diameter have been observed with Environmental Scanning Electron Microscopy (ESEM) as described below.

Black soot shows a stronger interaction with $H_2O$ vapor compared to gray soot, according to its higher $E_d$ value. Surprisingly, however, the $A_d$ factor for $H_2O$ vapor adsorption on both gray and black soot is lower by a factor of $10^4$ compared to expected values that are of the order of $10^{13}$ s$^{-1}$ for desorption processes whose values may commonly be found in the literature[50-52] for first-order desorption processes. However, such low $A_d$ factors have been measured in the past and may indicate an entropic bottleneck that may be explained by a fast preequilibrium controlled by an entropically unfavorable step such as surface diffusion, which we are unable to experimentally resolve given the present technique.

In agreement with the unusually low values of $A_d$ for $H_2O$ desorption the absolute values of $\tau_s$ are higher by the same amount in comparison to expected values from theory. We note that the presented values for $\tau_s$ are larger by four to six decades compared to an estimate given by Kärcher et al.,[26] who base their conclusion on experimental results of water adsorption on graphite which has a similar enthalpy change compared to soot examined here. The value of $\tau_s$ given by Kärcher et al.[26] is estimated by means of statistical mechanics and is related to the loss of entropy upon adsorption from the vapor state. Therefore, it does not constitute an experimentally measured absolute value as is the case in the present study. The fact that we are able to measure absolute values of $\tau_s$ is a consequence of the real-time kinetics performed in the present experiments.

Very little information exists on the hydration properties of aviation soot from a fundamental point of view. In the initial stages, soot from an internal combustion engine is expected to be hydrophobic, that is non-wettable.[31,53] However, a few qualitative experiments have been performed[29,30,46] which show that "*n*-hexane soot", carbonaceous particles, or aircraft combustor soot may become partially hydrated under certain conditions. Recently, Gorbunov et al.[33] have shown that the ice nucleation ability of soot aerosols is mainly influenced by the particle size and the surface concentration of functional groups that are able to form hydrogen bonds with water molecules by observing ice particle formation in a cloud chamber. We would like to point out that the molecular viewpoint of $H_2O$ adsorption on soot as presented here is in disagreement with the picture obtained from contact angle measurements with the sessile drop technique, which addresses a property of bulk water interacting with a macroscopic interface. We believe that the activation of the soot interface in the presence of $H_2O$ vapor at low temperatures has to be addressed on a molecular level such as used in this work.

**Influence of the Presence of Sulfur in Soot Samples on the Interaction $H_2O$/Soot.** In contrast to the belief that soot particles should be activated exclusively by $H_2SO_4$[8,26,28-31,54] to become hydrophilic, we show in the following that flame soot contains active surface sites for $H_2O$ adsorption in sufficient numbers in what seems to be a sulfur (S)-free pathway for $H_2O$ adsorption on fresh soot. Field observations of the number density of soot aerosol as a function of contrail age resulted in strong evidence that a significant fraction of soot aerosol, say roughly $^1/_3$, yielded ice nuclei without the incidence of sulfuric acid, which thus constitutes indirect evidence for a S-free pathway to contrail formation based on soot as condensation nuclei for atmospheric ice particles.[28,32] Similar conclusions have been reached from Cirrus observations[3] as well as from laboratory work cited above and in ref 55.

We first embarked on a baseline experiment to quantitatively measure the potential presence of sulfur compounds adsorbed

**TABLE 5: Arrhenius Parameters for the Desorption Rate Constant $k_d$ of H₂O Adsorbed on Soot**

| type of soot | $T$ [K] | $\tau_s$ [ms] | $\gamma_0$ | $10^{12}n_s$ [cm⁻²] | $E_a{}^c$ [kcal/mol] | $\log A_d{}^c$ [s⁻¹] |
|---|---|---|---|---|---|---|
| gray soot[a] | 298 | $0.3 \pm 0.2$ | $\leq 5 \times 10^{-4}$ | $12 \pm 2$ | $7.0 \pm 0.5$ | $8.8 \pm 0.5$ |
| | 243 | $4 \pm 1$ | $\leq 2 \times 10^{-3}$ | $16 \pm 2$ | | |
| | 193 | $160 \pm 100$ | $\leq 2 \times 10^{-3}$ | $20 \pm 2$ | | |
| black soot[b] | 298 | $15 \pm 5$ | $< 5 \times 10^{-4}$ | $30 \pm 10$ | $9.0 \pm 0.6$ | $8.5 \pm 0.5$ |
| | 263 | $125 \pm 50$ | $\leq 1 \times 10^{-3}$ | $30 \pm 10$ | | |
| | 243 | $400 \pm 100$ | $\leq 1 \times 10^{-3}$ | $30 \pm 10$ | | |

[a] $1.1 \times 29.5$ cm² tube. [b] $1.1 \times 20$ cm² tube. [c] The first-order rate constant for desorption of H₂O from flame soot is expressed as $k_d = A_d \exp(-E_d/RT)$ with $R = 1.987 \times 10^{-3}$ kcal mol⁻¹ K⁻¹.

**TABLE 6: Estimation of the Tube Portion in Which the H₂O Saturation Pressure Is Reached during a Diffusion Tube Experiment**

| $T$ [K] | $P_{sat,H_2O}$ [Pa] | $V_{sat}{}^a$ [cm³] | dist$_{(2\ cm\ dia)}{}^b$ [cm] | dist$_{(1.1\ cm\ dia)}{}^b$ [cm] | $\bar{c}{}^c$ [m/s] | $t_{sat(1.1\ cm\ dia)}{}^d$ [ms] |
|---|---|---|---|---|---|---|
| 298 | 3159.55 | $1.3 \times 10^{-3}$ | $4.1 \times 10^{-4}$ | 0.0014 | 594.2 | $2.35 \times 10^{-5}$ |
| 243 | 38.02 | $8.82 \times 10^{-2}$ | 0.028 | 0.093 | 536.6 | $1.73 \times 10^{-3}$ |
| 193 | 0.0532 | 5.0 | 1.59 | 5.26 | 478.3 | 0.11 |

[a] $V^{sat} = N/P_{sat} \cdot RT$, with $N = 1.66 \times 10^{-9}$ mol corresponding to a dose of $10^{15}$ molecules and $R = 8.31$ J mol⁻¹ K⁻¹. [b] Distance from the injection point where $P_{H_2O} = P_{sat,H_2O}$ for the 2.0 and 1.1 cm diameter tube, respectively. [c] $\bar{c} = \sqrt{(8RT/\pi M)}$, with $M = 18$. [d] Time during which $P_{H_2O} \geq P_{sat,H_2O}$ in the 1.1 cm diameter tube.

on nominally S-free decane soot. The thinking behind this experiment was to investigate whether the H₂O adsorption properties on decane soot observed so far (Tables 3 and 4) were the result of significant amounts of adsorbed H₂SO₄ originating from traces of S present in the used decane fuel. The experimental procedure consists of extracting a sample of gray decane soot in methanol followed by the analysis of the soot extraction by ion chromatography (IC) for its sulfate (SO₄²⁻) and by ICP for its total S-content. The quantities extracted indicated upper limits of $3.4 \times 10^{-4}$ and $4 \times 10^{-4}$ of a monolayer of sulfate (IC) and total S (ICP), respectively, using the measured BET surface area of 69 m² g⁻¹ for gray decane soot.[39] These coverages are identical within experimental error and correspond to 4−6% of the total available surface sites $n_s$ of the extracted gray soot sample (column 5 of Table 3). In addition, all sulfur species are speciated as adsorbed sulfate leaving no room for S-species other than S(VI). The conclusion is that negligible amounts of sulfur are adsorbed on gray flame soot generated from nominally sulfur-free decane despite a potentially significant S-content in decane fuel, which was not analyzed in this work. We may add that although the quantity of water adsorbing on soot was generally expected to strongly depend on the soot sulfur content,[31] to our knowledge no experiments have been undertaken so far to investigate the quantity of sulfur species adsorbed on soot. However, several observations of airplane contrail formation with fuel of high (up to 5500 ppm mass fraction) and low (a few ppm, essentially S-free) S-content[8,56] have been made, but without investigating how much H₂SO₄ was in fact adsorbed on the emitted soot particles. In most of these cases a high number of volatile H₂SO₄ aerosol particles were present in the gas phase[13] enabling heterogeneous ice nucleation on liquid or frozen sulfuric acid aerosol particles. In addition, Arnold and co-workers have found small electrically charged soot particles that are emitted from the exhaust of an aircraft gas-turbine engine combustor that may indirectly alter the condensation and nucleation rates in the presence of soot.[57]

To test the effect of the fuel sulfur content (FSC) on the H₂O adsorption properties of the resulting soot we have also performed experiments in which gray and black soot have been generated from the combustion of decane fuel containing either 50 or 500 ppm (by weight) of thiophene (C₄H₄S). The intent was to test the influence of FSC regarding the H₂O adsorption capability of the resulting flame soot owing to the possible

presence of S-containing species, presumably H₂SO₄, adsorbed on the soot sample. A comparison between raw MS signals with thiophene-free and thiophene spiked black decane soot is illustrated in Figure 8. Table 7 summarizes the experiments performed with gray and black decane soot spiked with known amounts of thiophene.

We may see in Figure 8 that H₂O adsorption experiments performed with thiophene-spiked decane fuel do not differ significantly from the ones performed with thiophene-free decane fuel at all temperatures at variance with previous studies.[22] This result may be compared to the observation on the formation of airplane contrails of Busen and Schumann,[56] who were not able to observe any visible difference in contrails formed by burning fuel containing 2 and 250 ppm sulfur. Nevertheless, further observations on airplane contrails made by Schumann et al.[8] demonstrated a small but measurable influence of FSC on contrail formation with use of a sulfur mass fraction of the jet fuel varying from 170 to 5500 ppm. The present studies show that a significant FSC of up to 500 ppm mass fraction will not have an impact on the H₂O adsorption properties of soot within the examined range of FSC in decane.

This negative result may indicate that a 500 ppm FSC in decane does not lead to significant deposition of H₂SO₄ onto the soot under the combustion conditions for the generation of black and gray decane soot. Conversely, had we observed an important change of the kinetic parameters of H₂O adsorption on decane soot at 500 ppm FSC, we would have been forced to conclude that a significant amount of H₂SO₄ had been deposited onto the soot during decane/thiophene combustion. Results of ancillary experiments[41] dealing with the study of the change of adsorbed sulfate with increasing FSC in the range 0 to 5000 ppm (by volume) carried out on hexane and octane soot revealed an extremely small conversion efficiency transforming FSC to adsorbed sulfate. For instance, this efficiency is of the order of $5 \times 10^{-4}$ in the range 50 to 5000 ppm of FSC present as thiophene for black and gray octane soot. We therefore conclude that at least for flame soot generated in a diffusion flame of decane/thiophene an exceedingly small percentage of the sulfur ends up adsorbed on the soot if we take the quantitative results obtained for black octane soot generation in a diffusion flame as an example close enough to decane. It is obvious that the future understanding of the FSC effect on aviation contrail formation depends on the careful analysis of aviation soot in regards to adsorbed H₂SO₄ or "sulfate".
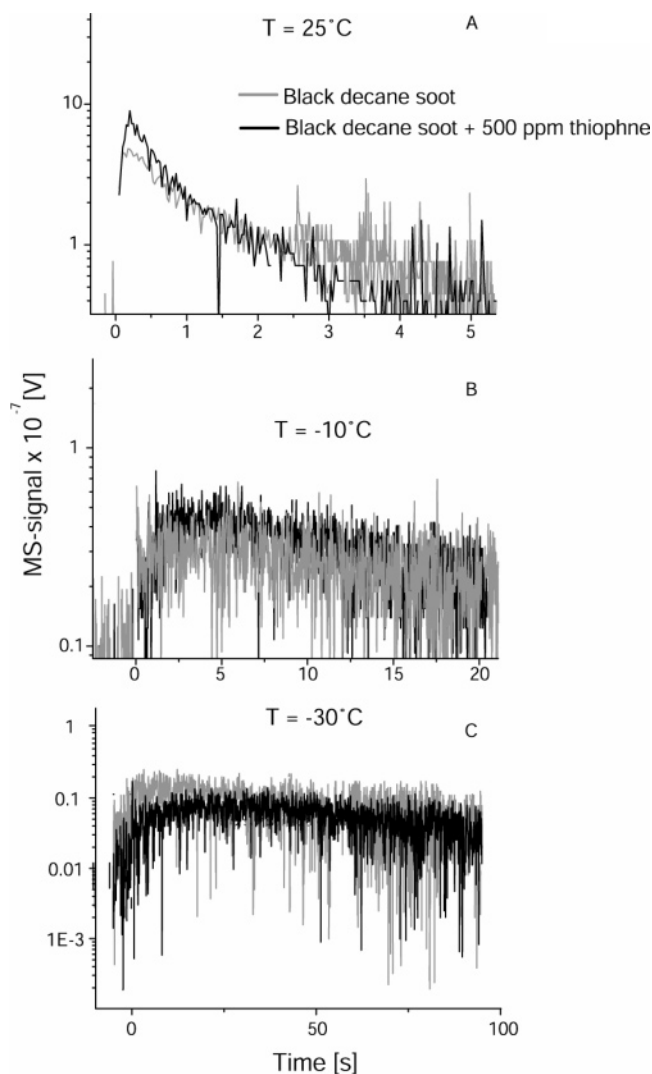
**Figure 8.** Experimental raw MS signals of $H_2O$ monitored at *m/e* 18 interacting with black decane soot (gray traces) and thiophene doped black decane soot (black traces: 500 ppm) at three different temperatures, $T = 25 \pm 2$, $-10$, and $-30$ °C. Experiments have been performed in a $1.1 \times 20$ cm$^2$ ($Z = 565$) tube with doses of $1.1 \times 10^{15}$ molecules.

**H₂O Saturation Experiments.** To test the saturation of the soot substrates with respect to adsorption of $H_2O$ vapor we have performed three types of experiments permitting the determination of the degree of $H_2O$ saturation of the soot surface as a function of the dose of injected $H_2O$ molecules as well as the time scale over which the saturation persists. The first type of experiment consisted of injecting pulses of $H_2O$ molecules at regular intervals of 60 s and observing the potential changes in the shape and integral of the signals. The second type of experiment consisted of interrogating the surface with a small pulse (probe pulse), then saturating the surface with a large pulse (saturation pulse) and finally testing the degree of surface saturation by firing again a probe pulse. The third type of experiment was performed to determine the time during which the saturation of the surface persists by measuring the recovery time of the original arrival time curve. It consists of saturating the soot surface with two or three large pulses and probing the state of the surface at different times until the signal recovers its initial shape, which corresponds to a nonsaturated signal.

The first type of experiment shown in Figure 9 for gray decane soot at 193 K has been performed by using a series of $H_2O$ pulses of $4.7 \times 10^{15}$ molecules injected at regular time

**TABLE 7: Kinetic Results of H₂O Interacting with Gray and Black Decane Soot over a Range of Temperatures and Spiked with Thiophene (C₄H₄S) of Varying Concentration**

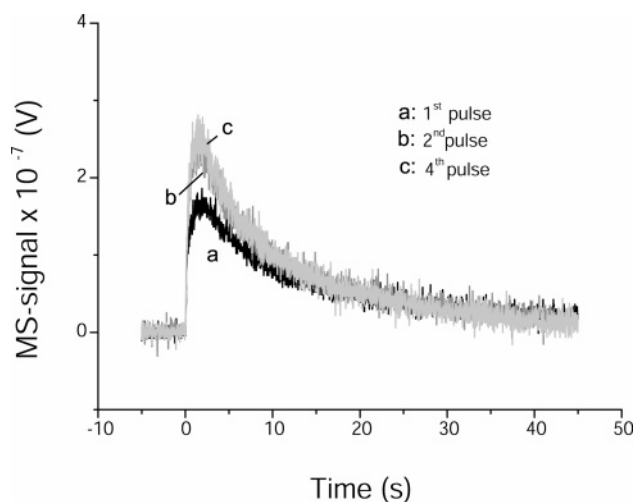| soot type | $T$ [°C] | concn of (C$_4$H$_4$S) [ppm] | dose$^a$/10$^{14}$ [molecule] | $\tau_s{}^m$ [s] | $10^{-2}\gamma^m$ |
|---|---|---|---|---|---|
| gray | 25 | 50 | 19 | 0.008 | 0 |
| | | 50 | 20 | 0.008 | 0 |
| | | 50 | 16 | 0.008 | 0 |
| | | 500 | 18 | 0.014 | 0 |
| | $-30$ | 50 | 19 | 0.061 | 0 |
| | | 50 | 20 | 0.051 | 0 |
| | | 50 | 20 | 0.051 | 0.05 |
| | | 50 | 16 | 0.021 | 0 |
| | $-80$ | 50 | 19 | 9 | 0.003 |
| | | 50 | 20 | 8.1 | 0.03 |
| | | 50 | 16 | 1.6−2.7 | 0.007 |
| | | 500 | 9 | 5.5 | 0.01 |
| | | 500 | 18 | 6.7 | 0.07 |
| black | 25 | 50 | 25 | 0.8 | 0 |
| | | 500 | 9.6 | 1.1 | 0 |
| | $-10$ | 50 | 25 | 17 | |
| | | 500 | 9.6 | 33 | 0 |
| | $-30$ | 50 | 25 | 60 | |
| | | 500 | 9.6 | 122 | |

$^a$ The uncertainty in the dose is 10−20%.



**Figure 9.** Experimental raw signals of $H_2O$ monitored at *m/e* 18 of a saturation experiment where $H_2O$ interacted with gray decane soot in pulses injected at intervals of 60 s into the diffusion tube ($1.1 \times 29.5$ cm$^2$, $Z = 1190$) at a temperature of 193 K. The dose was $4.7 \times 10^{15}$ molecules.

intervals of 60 s. We observe that already the second pulse fired 60 s after the first one shows saturation behavior, which is visible in the higher number of early arriving molecules. The following pulses such as the 3rd, 4th, and the following are equivalent to the second pulse showing the same degree of saturation. This behavior has been observed for both gray and black decane soot.

The second type of experiment consisted of successively injecting a probe ($1.4 \times 10^{15}$ molecules), a saturation ($4.7 \times 10^{15}$ molecules), and again a probe pulse to compare the shape and integrals of the two $H_2O$ probe pulses. The results of these experiments are illustrated in Figure 10, which presents a comparison of the small probe pulses obtained as explained above for gray (panel A) and black soot (panel B) at 193 and 243 K, respectively. This experiment shows that a large pulse of $4.7 \times 10^{15}$ $H_2O$ molecules is sufficient to saturate the soot surface. The second probe pulse fired 6 min after the saturation pulse shows saturation characteristics corresponding to a sharper and an earlier peak, which means that a larger amount of
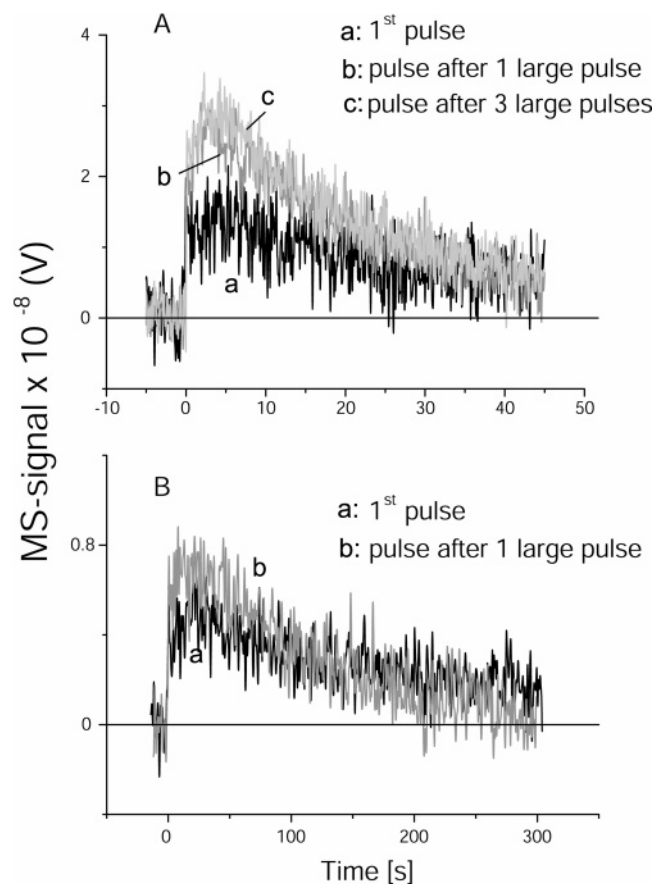
**Figure 10.** Comparison between two small probe pulses of H$_2$O (1.4 × 10$^{15}$ molecules) in a saturation experiment where H$_2$O interacted with gray (panel A) and black (panel B) decane soot before and after the introduction of a large H$_2$O saturation pulse (4.7 × 10$^{15}$) into the tube. Pulses of panel A (gray soot) have been fired at intervals of 1 min within a 1.1 × 29.5 cm$^2$ tube ($Z = 1190$) and at $T = 193$ K. Panel B represents pulses on black decane soot at $T = 243$ K fired at intervals of 6 min in a 1.1 × 20 cm$^2$ tube ($Z = 565$).
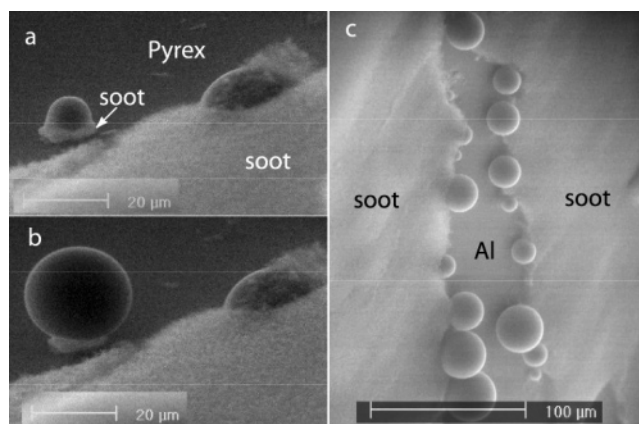
**Figure 11.** ESEM pictures of water drops grown on a black decane soot substrate at 100% relative humidity at 277 K. Panels a and b represent the growth of a water drop on a soot patch deposited on a Pyrex substrate as a function of time, whereas panel c shows the development of water drops on the walls of a crack in the soot layer deposited on an aluminum substrate. No droplets are formed on the bare aluminum substrate whereas they grow on the coldest part of the soot layer, which is closest to the substrate.

surviving H$_2$O molecules arrives during the first few seconds because the saturation of gray and black soot persists on the time scale of 1 and 6 min, respectively, at low temperatures.

The third type of experiment has been performed to determine the time necessary for soot to regenerate, that is the time after which a transient MS signal regains the same shape as the original probe MS signal after saturation of the soot sample by the large H$_2$O pulse. From this last series of experiments we have determined that the soot surface is regenerated after approximately 10 and 15 min for gray soot at $T = 193$ and black soot at $T = 243$ K, respectively, owing to desorption of adsorbed H$_2$O molecules. The sample may thereafter regain the status of fresh soot surface ready for further H$_2$O adsorption.

In conclusion of the saturation experiments we may state that gray and black decane soot substrates show signs of saturation at low temperatures when they are exposed to successive pulses at doses larger than 4.7 × 10$^{15}$ molecules. This manifests itself in a higher number of H$_2$O molecules effusing out earlier of the diffusion tube compared to an initial pulse on fresh soot owing to a weaker interaction of H$_2$O with surface sites already occupied by H$_2$O molecules from the previous pulse. In fact, at the end of the second pulse of 4.7 × 10$^{15}$ molecules all adsorption sites on the soot seem to be already saturated. Each successive H$_2$O pulse therefore interacts with a totally saturated surface. Moreover, we did not observe any loss of H$_2$O on a saturated soot substrate compared to the initial interaction of H$_2$O vapor with a fresh soot substrate in agreement with

saturation of all adsorption sites. In support of this, the integrals of successive pulses tend to slightly increase when pulses are fired at short time intervals because desorbing molecules from previous pulses are detected at the same time as H$_2$O from the pulse under consideration. In this way more H$_2$O molecules than are contained in the original dose may be detected after firing a pulse on a saturated soot substrate.

The rate of regeneration of a soot surface saturated with water is faster for gray than for black soot with regeneration times of 10 and 15 min at 193 and 243 K, respectively. Nevertheless, growth of water droplets or ice crystals has not been observed under the present experimental conditions as expected because the partial pressure of H$_2$O in the diffusion tube during a pulsed valve experiment is not high enough to correspond to supersaturation conditions as shown in Table 6. The adsorbed H$_2$O molecules desorb too rapidly to allow a persistent adsorption of H$_2$O vapor on already adsorbed H$_2$O molecules, which is the reason a raw MS signal once saturated does not change its shape with further consecutive pulses. However, the growth of water droplets on black decane soot has been observed with electron microscopy at a relative humidity of 100% as explained below.

**Observation of Water Droplet Formation on Black Decane Soot with Environmental Secondary Electron Microscopy (ESEM).** Additional supporting observations have been made with use of an environmental electronic microscope (Philips XL30 ESEM-FEG) at 100% relative humidity (rh), using a black decane soot substrate deposited on a suitable support such as Al and Pyrex. At 277 K and 100% rh we have observed the appearance of water drops on soot with a diameter of several tens of a micrometer as displayed in Figure 11a,b,c. These drops always grew where the soot layer was thinnest, that is coldest, because of its proximity to the cooling support, either on a small soot patch deposited on a Pyrex substrate (Figure 11a,b) or on the coldest part of the side walls of a crack in the soot substrate close to the aluminum substrate (Figure 11c). These images suggest that fresh soot may offer adsorption sites for H$_2$O vapor leading to the appearance of bulk H$_2$O under the proper supersaturation conditions. Interestingly enough, in not a single case have we observed growth of water droplets on the support material of Al or Pyrex[42] whose molecular surface consists of Al$_2$O$_3$ and mostly SiO$_2$ together with oxides of B, K, and Na,

**TABLE 8: Estimated Rates of Adsorption $R_a$ and Desorption $R_d$ of $H_2O$ from Combustion Aerosol Emitted from an Aircraft Engine Approximated by Gray and Black Soot at Atmospheric Conditions**

| | 700 K | 500 K | 281 K | 237 K | 223 K |
|---|---|---|---|---|---|
| distance behind nozzle [m] | 0 | 0 | 1.5 | ~200 | ∞ (background) |
| $\bar{c}^a$ [cm s$^{-1}$] | $9.1 \times 10^4$ | $7.7 \times 10^4$ | $5.7 \times 10^4$ | $5.3 \times 10^4$ | $5.1 \times 10^4$ |
| $H_2O^b$ (g) [molecules cm$^{-3}$] | $3.1 \times 10^{16}$ | $4.3 \times 10^{16}$ | $7.6 \times 10^{16}$ | $8.4 \times 10^{15}$ | $2.1 \times 10^{15}$ |
| $S/V^c$ [cm$^{-1}$] | $5 \times 10^{-5}$ | $5 \times 10^{-5}$ | $5 \times 10^{-5}$ | $1 \times 10^{-5}$ | $3 \times 10^{-10}$ |
| $k_a^d = \omega$ [s$^{-1}$] | 1.13 | 1 | 0.7 | 0.13 | $3.8 \times 10^{-10}$ |
| $R_a^d$ [molecules cm$^{-3}$ s$^{-1}$] | $3.5 \times 10^{16}$ | $4.3 \times 10^{16}$ | $5.3 \times 10^{16}$ | $1.1 \times 10^{15}$ | $8.0 \times 10^9$ |
| $k_d^e$ [s$^{-1}$] (gray) | $4.1 \times 10^6$ | $5.5 \times 10^5$ | $2.3 \times 10^3$ | $2.2 \times 10^2$ | $8.7 \times 10^1$ |
| $k_d^f$ [s$^{-1}$] (black) | $4.9 \times 10^5$ | $3.7 \times 10^4$ | 31.6 | 1.6 | 0.48 |
| $R_d^g$ [molecules cm$^{-3}$ s$^{-1}$] (gray) | $4.1 \times 10^{16}$ | $5.5 \times 10^{15}$ | $2.3 \times 10^{13}$ | $4.4 \times 10^{11}$ | $5.2 \times 10^6$ |
| $R_d^g$ [molecules cm$^{-3}$ s$^{-1}$] (black) | $4.9 \times 10^{15}$ | $3.7 \times 10^{14}$ | $3.2 \times 10^{11}$ | $3.2 \times 10^9$ | $2.9 \times 10^4$ |

$^a$ $\bar{c} = [(8 \times 8.31 \times T)/(\pi \times 0.018)]^{0.5} \times 100$ cm s$^{-1}$. $^b$ $H_2O$ (g) calculated from $P_{H_2O} = 30$ Pa at 237 K, 7 Pa at 223 K. The $H_2O$ partial pressure was assumed to be invariant in the range 700 to 281 K and equal to $7.6 \times 10^{16}$ molecules cm$^{-3}$ at 281 K (1.5 m behind the exit nozzle). No dilution of $H_2O$ vapor was assumed between 0 and 1.5 m behind the exit nozzle. $^c$ No dilution of soot aerosol between 0 and 1.5 m was assumed. $^d$ $k_a = (\bar{c}/4)(S/V)$. This corresponds to the maximum theoretically allowed rate constant in agreement with an uptake coefficient of unity and is numerically equal to the gas-substrate collision frequency $\omega$. $^e$ $k_d = 10^{8.8}$ e$^{(-7000/1.987T)}$. $^f$ $k_d = 10^{8.5}$ e$^{(-9000/1.987T)}$. $^g$ $R_d = k_d(S/V)(H_2O(ads))$, with $H_2O$(ads) = $2 \times 10^{14}$ molecules cm$^{-2}$ as an upper limit.

respectively. We conclude that in the given competitive situation soot is more highly activated in regards to the growth of $H_2O$ droplets than the inorganic oxides of the support material. We thereby assume that the prerequisite for the activation of droplet formation is prior molecular adsorption of $H_2O$ vapor on appropriate adsorption sites.

**Atmospheric Significance of the Kinetic Results.** We have shown that $H_2O$ has a surface residence time $\tau_s$ on soot in the range of a few to several hundreds of milliseconds depending on temperature and type of soot. If we consider a specific case of an airplane trajectory assuming a surface area density ($S/V$) of soot in the plume of $5 \times 10^{-5}$ cm$^2$/cm$^3$ close to the nozzle exit of the airplane[21,58] and a water concentration of $7.6 \times 10^{16}$ molecules cm$^{-3}$ at a temperature of 281 K at 1.5 m behind the engine nozzle,[21] we may calculate the (maximum) rate of $H_2O$ adsorption $R_a = 5.3 \times 10^{16}$ molecule cm$^{-3}$ s$^{-1}$ compared to the rate of $H_2O$ desorption $R_d = 2.3 \times 10^{13}$ and $3.2 \times 10^{11}$ molecule cm$^{-3}$ s$^{-1}$ for gray and black soot, respectively (see Table 8). This indicates that already a few meters behind the engine nozzle aviation soot may be covered by adsorbed $H_2O$ owing principally to the exponential drop in $R_d$ with decreasing temperature. At 200 m behind the airplane both the soot concentration and $H_2O$ partial pressure drop to $10^{-5}$ cm$^2$/cm$^3$ [21,58] and 30 Pa at 237 K, respectively. These values have been measured for a persistent contrail generated by a B-747 aircraft.[28] At this point $R_a = 1.1 \times 10^{15}$, $R_d = 4.4 \times 10^{11}$ and $3.2 \times 10^9$ molecule cm$^{-3}$ s$^{-1}$ for gray and black soot, respectively. It is apparent that the net rate of $H_2O$ adsorption on soot increases with plume age and thus distance from the engine. Even for atmospheric background conditions of $T = 223$ K, a $H_2O$ partial pressure of 7 Pa,[28] and a soot concentration of $3 \times 10^{-10}$ cm$^2$/cm$^3$,[21,58] we calculate $R_a = 8.0 \times 10^9$, $R_d = 5.2 \times 10^6$ and $2.9 \times 10^4$ molecule cm$^{-3}$ s$^{-1}$ for gray and black soot, respectively. This supports the important conclusion that soot is covered by adsorbed $H_2O$ even at background conditions owing to the low temperatures. The temperature at which $R_a$ approaches $R_d$ corresponds to 700 K if soot aerosol resembles black soot or 500 K for gray soot. This means that already within a few meters behind the exit nozzle soot is coated with an adsorbed $H_2O$ layer, which persists under background conditions as well. Once the soot has a hydrophilic coating or $H_2O$ clusters adsorbed to it, it is presumably activated and able to continue to function as an ice nucleating agent finally leading to ice particles if the atmospheric humidity satisfies the Appleman criterion.[7] We therefore postulate that fresh soot may partake in the formation of aircraft contrails or may induce the formation of Cirrus clouds at a later point in time in a sulfur-free process,

away from the aircraft corridor under appropriate supersaturation conditions.

$H_2O$ interacting with soot constitutes a complex physicochemical system, which includes interactive processes and saturable adsorption. The one-site Monte Carlo model has been applied to fit the experimental signals corresponding to a complex decay and to determine the kinetic parameters: they are the uptake coefficient $\gamma_0^{MC}$, the surface residence time $\tau_s$, and the number of adsorption sites $n_s$. The model takes into account adsorption prior to reaction as well as surface saturation. In fact, the saturation that occurs during an individual pulse is responsible for the nonexponential decay of the MS signal. Experimental arrival times have successfully been simulated for all soot samples generated from liquid fuels in the simple burner as well as in the Bunsen burner for acetylene soot. The interaction of $H_2O$ with soot at $298 \pm 2$ K as expressed by the kinetic results for soot produced by combustion of two liquid (toluene, diesel) and one gaseous fuel (acetylene) are very similar. However, decane soot produced in the simple burner seems to interact more weakly with water and constitutes an exception among the four tested types of soot. At $298 \pm 2$ K initial uptake coefficients $\gamma_0^{MC}$ of $H_2O$ on toluene, acetylene, and diesel soot are lower than $2 \times 10^{-3}$ and residence times $\tau_s$ up to 5 ms have been measured.

The study of two types of decane soot originating from a lean (black soot) and a rich (gray soot) flame, as a function of temperature, shows surface residence times $\tau_s$ of adsorbed $H_2O$ which increase with decreasing temperature. In fact, $\tau_s$ increases from $\tau_s = 0.3 \pm 0.2$ ms at $T = 298$ K to $\tau_s = 160 \pm 100$ ms at $T = 193$ K for gray decane soot and from $\tau_s = 15 \pm 5$ ms at $T = 298$ K to $\tau_s = 400 \pm 100$ ms at $T = 243$ K for black decane soot. The Monte Carlo simulation model is consistent with an uptake coefficient $\gamma_0^{MC}$ and a number of adsorption sites $n_s$ per cm$^2$ which are essentially temperature independent. Therefore, we may claim that all the observed variation in the interaction between $H_2O$ and decane soot as a function of temperature is absorbed in the parameter $\tau_s$ or the desorption rate constant $k_d$ of reaction 3. Surface adsorption sites $n_s$ are larger by a factor of 2–3 for black compared to gray decane soot, but represent only 1% of a pure amorphous carbon surface, which contains approximately $2 \times 10^{15}$ C atoms per cm$^2$. Therefore, we postulate that $H_2O$ adsorption occurs either on surface defects or on impurities of soot or surface functional groups, which are able to form hydrogen bonds with water molecules. We discard the possibility that the observed values of $\tau_s$ may result from the sampling of potential micropores present in our soot samples because $\tau_s$ shows an exponential

Interaction of H₂O Vapor with Soot

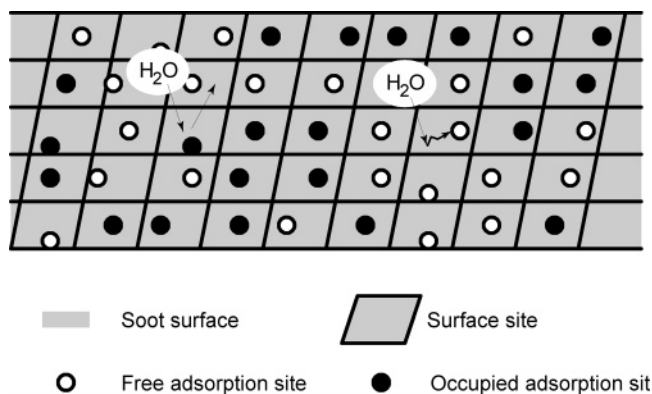*J. Phys. Chem. A, Vol. 108, No. 48, 2004* **10679**



**Figure 12.** Cartoon of the Monte Carlo model applied to the interaction of $H_2O$ on soot. Every collision of $H_2O$ with the soot surface occurs with a grid cell containing a surface site. If the adsorption site of the surface is busy, the molecule bounces off the surface site immediately. When the adsorption site is free the molecule migrates to the adsorption site and stays adsorbed during the residence time $\tau_s$ before desorbing.

dependence with temperature $(\exp(1/T))$ and does not follow a $1/T^{1/2}$ law that would result from a decrease of the molecular mean velocity $c$ with decreasing temperature. Owing to the extended temperature range of the present study we may assert this conclusion with some confidence.

The Monte Carlo model used to fit the arrival times with the kinetic parameters $\tau_s$, $n_s$, and $\gamma_0$ for the interaction of $H_2O$ and decane soot is relatively simple but succeeds surprisingly well in describing all the observables. The situation may be summarized as follows: The cross section of a surface site is large enough so that every collision of the $H_2O$ molecule occurs with a surface site. In other words, the surface of the sample is divided by a grid whose cells represent surface sites for a potential $H_2O$ adsorption (see Figure 12). Each surface site possesses on average one adsorption site, which corresponds to a surface defect, an impurity, or a functional group. If the adsorption site is free, the water molecule stays on the surface site during a time equal to the residence time $\tau_s$ before desorbing. During the residence time the molecules migrate on the surface to find the adsorption site in order to adsorb. Once the molecule has collided with a free surface site we may not distinguish if the residence time $\tau_s$ is the time the molecule needs to find the adsorption site or if it is the time during which the molecule stays adsorbed on it because the present experiments are "blind" to elementary processes occurring on surface sites. This is tantamount to stating that the present experiments are unable to resolve the kinetics of surface diffusion processes. In the other case, when the adsorption site is already occupied by a $H_2O$ molecule, the incoming molecule bounces off the surface site immediately. In this model the area of a surface site depends on the type of soot. It varies from 5 to 8.33 nm² for gray soot deposited in a 1.1 × 29.5 cm² tube $(n_s = (12-20) \times 10^{12}$ cm⁻², see Table 5) and is about 3.3 nm² for black decane soot in a 1.1 × 20 cm² tube $(n_s = 30 \times 10^{12}$ cm⁻², see Table 5), which corresponds to approximately 140−230 C atoms per surface site for gray soot and 80 C atoms for black soot, considering that a C atom occupies $3.6 \times 10^{-16}$ cm², which has been calculated by using the density of amorphous carbon of 1.8 g/cm³.

The used Monte Carlo model assumes that every collision of the $H_2O$ molecule with the soot surface may lead to adsorption, which means that the accommodation coefficient $\alpha$ assumed in this work is equal to 1. Unfortunately, we cannot verify this fact experimentally, which would require a single collision experiment. However, an $\alpha$ value smaller than 1 would

mean surface residence times $\tau_s$ larger than the present ones, because the delay in the arrival time of the MS signal measured in the $H_2O$−decane soot interactions leading to adsorption would be the result of a lower number of collisions. This in turn would mean a proportionally longer residence time per collision leading to adsorption, which would lead to an even lower $A$ factor for $H_2O$ desorption. We may therefore claim that the present $\tau_s$ values represent a lower limit for the case that $\alpha \leq 1$ and that the $A_d$ factors for desorption of $H_2O$ are upper limits to the true values.

**References and Notes**

(1) Houghton, J. T.; Ding, Y.; Griggs, D. J.; Noguer, M.; van den Linden, P. J.; Dai, X.; Maskell, K.; Johnson, C. A. *Climate Change 2001: The Scientific Basis*; Intergovernmental Panel on Climate Change (IPCC); Cambridge University Press: Cambridge, 2001.

(2) Schwartz, S. E. *J. Aerosol Sci.* **1996**, *27*, 359.

(3) Jensen, E. J.; Toon, O. B. *Geophys. Res. Lett.* **1997**, *24*, 249.

(4) Gierens, K.; Schumann, U.; Helten, M.; Smit, H.; Wang, P. H. *J. Geophys. Res.* **2000**, *105*, 22743.

(5) Jensen, E. J.; Toon, O. B.; Vay, S. A.; Ovarlez, J.; May, M.; Bui, T. P.; Twohy, C. H.; Gandrud, B. W.; Pueschel, R. F.; Schumann, U. *J. Geophys. Res.* **2001**, *106*, 17253.

(6) Schumann, U. In *Cirrus*; Lynch, D. K., Sassen, K., Starr, D. O'C., Stephens, G., Eds.; Oxford University Press: Oxford, UK, 2002.

(7) Appleman, H. *Bull. Am. Meteorol. Soc.* **1953**, *34*, 14.

(8) Schumann, U.; Ström, J.; Busen, R.; Baumann, R.; Gierens, K.; Krautstrunk, M.; Schröder, F. P.; Sting, J. *J. Geophys. Res.* **1996**, *101*, 6853.

(9) McDonald, J. E. *J. Geophys. Res.* **1965**, *70*, 1553.

(10) Boucher, O. *Nature* **1999**, *397*, 30.

(11) Zerefos, C. S.; Eleftheratos, K.; Balis, D. S.; Zanis, P.; Tselioudis, G.; Meleti, C. *Atmos. Chem. Phys.* **2003**, *3*, 1633.

(12) Miake-Lye, R. C.; Anderson, B. E.; Cofer, W. R.; Wallio, H. A.; Nowicki, G. D.; Ballenthin, J. O.; Hunton, D. E.; Knighton, W. B.; Miller, T. M.; Seeley, J. V.; Viggiano, A. A. *Geophys. Res. Lett.* **1998**, *25*, 1677.

(13) Arnold, F.; Stilp, Th.; Busen, R.; Schumann, U. *Atmos. Environ.* **1998**, *32*, 3073.

(14) Schumann, U.; Schlager, H.; Arnold, F.; Baumann, R.; Harschbarger, P.; Klemm, O. *Atmos. Environ.* **1998**, *32*, 3097.

(15) Gierens, K.; Ström, J. *J. Atmos. Sci.* **1998**, *55*, 3253.

(16) Penner, J. E.; Lister, D. H.; Griggs, D. J.; Dokken, D. J.; McFarland, M. *Aviation and the global atmosphere*; Published for the Intergovernmental Panel on Climate Change (IPCC); Cambridge University Press: Cambridge, 1999; p 87.

(17) Kuhn, M.; Petzold, A.; Baumgardner, D.; Schröder, F. P. *Geophys. Res. Lett.* **1998**, *25*, 2679.

(18) Sheridan, P. J.; Brock, C. A.; Wilson, J. C *Geophys. Res. Lett.* **1994**, *21*, 2587.

(19) Penner, J. E.; Heff, D.; Leaitch, R. *Environ. Sci. Technol.* **2001**, 332A.

(20) Blake, D. F.; Kato, K. *J. Geophys. Res.* **1995**, *100*, 7195.

(21) Petzold, A.; Döpelheuer, A.; Brock, C. A.; Schröder, F. *J. Geophys. Res.* **1999**, *104*, 22171.

(22) Lammel, G.; Novakov, T. *Atmos. Environ.* **1995**, *29*, 813.

(23) Diehl, K.; Mitra, S. K. *Atmos. Environ.* **1998**, *32*, 3145.

(24) Studebaker, M. L.; Snow, C. W. *J. Phys. Chem.* **1955**, *59*, 973.

(25) Schrader, M. *J. Phys. Chem.* **1975**, *79*, 2508.

(26) Kärcher, B.; Peter, Th.; Biermann, U. M.; Schumann, U. *J. Atmos. Sci.* **1996**, *53*, 3066.

(27) deMott, P. J.; Chen, Y.; Kreidenweis, S. M.; Rogers, D. C.; Sherman, D. E. *Geophys. Res. Lett.* **1999**, *26*, 2429.

(28) Kärcher, B.; Busen, R.; Petzold, A.; Schröder, F. P.; Schumann, U.; Jensen, E. J. *J. Geophys. Res.* **1998**, *103*, 17129.

(29) Chughtai, A. R.; Miller, N. J.; Smith, D. M.; Pitts, J. R. *J. Atmos. Chem.* **1999**, *34*, 259.

(30) Chughtai, A. R.; Miller, N. J.; Smith, D. M.; Pitts, J. R. *Atmos. Environ.* **1999**, *33*, 2679.

(31) Wyslouzil, B. E.; Carleton, K. L.; Sonnenfroh, D. M.; Rawlins, W. T.; Arnold, S. *Geophys. Res. Lett.* **1994**, *21*, 2107.

(32) Schröder, F.; Kärcher, B.; Duroure, C.; Ström, J.; Petzold, A.; Gayet, J. F.; Strauss, B.; Endling, P.; Borrmann, S. *J. Atmos. Sci.* **2000**, *57*, 464.

(33) Gorbunov, B.; Baklanov, A.; Kakutkina, N.; Windsor, H. L.; Toumi, R. *Aerosol Sci.* **2001**, *32*, 199.

(34) Popovitcheva, O. B.; Persiantseva, N. M.; Trukhin, M. E.; Rulev, G. B.; Shonija, N. K.; Buriko, Yu. Ya.; Starik, A. M.; Demirdjian, B.; Ferry, D.; Suzanne, J. *Phys. Chem. Chem. Phys.* **2000**, *2*, 4421.

(35) Ferry, D.; Suzanne, J. *J. Geophys. Res.* **2002**, *107*, 4734.

(36) Alcala-Jornod, C.; van den Bergh, H.; Rossi, M. J. *Geophys. Res. Lett.* **2002**, *29*, 1820; doi 10.1029/2001GL014115.

(37) Koch, T. G.; Fenter, F. F.; Rossi, M. J. *Chem. Phys. Lett.* **1997**, *275*, 253.

(38) Koch, T. G.; Rossi, M. J. *J. Phys. Chem.* **1998**, *102*, 9193.

(39) Stadler, D.; Rossi, M. J. *Phys. Chem. Chem. Phys.* **2000**, *2*, 5420.

(40) Salgado-Munoz, M. S.; Rossi, M. J. *Int J. Chem. Kinet.* **2002**, *34*, 620.

(41) Ngouabé Tchokotcha, N.; Rossi, M. J. In preparation, 2004.

(42) Alcala-Jornod, C. Ph.D. Thesis No. 2655, Ecole Polytechnique Fédérale de Lausanne (EPFL), 2002.

(43) Alcala-Jornod, C.; van den Bergh, H.; Rossi, M. J. *Phys. Chem. Chem. Phys.* **2000**, *2*, 5584.

(44) Koch, T. G.; Rossi, M. J. *Phys. Chem. Chem. Phys.* **1999**, *1*, 2687.

(45) Garten, V. A.; Head, R. B. *Nature* **1964**, *205*, 160.

(46) Chughtai, A. R.; Brooks, M. E.; Smith, D. M. *J. Geophys. Res.* **1996**, *101*, 19505.

(47) Chaix, L.; van den Bergh; H.; Rossi, M. J. *J. Phys. Chem. A* **1998**, *102*, 10300.

(48) Delval, C.; Flückiger, B.; Rossi, M. J. *Atmos. Chem. Phys.* **2003**, *3*, 1131.

(49) Marti, J.; Mauersberger, K. *Geophys. Res. Lett.* **1993**, *20*, 363.

(50) Seebauer, E. G.; Kong, A. C. F.; Schmidt, L. D. *Surf. Sci.* **1988**, *193*, 417.

(51) Madix, R. J. *Surf. Sci.* **1993**, *299/300*, 785.

(52) Carlsson, A. F.; Madix, R. J. *J. Phys. Chem. B* **2001**, *105*, 3261.

(53) Müller, E. A.; Rull, L. F.; Vega, L. F.; Gubbins, K. E. *J. Phys. Chem.* **1996**, *100*, 1189.

(54) Whitefield, P. D.; Trueblood, M. B.; Hagen, D. E. *Part. Sci. Technol.* **1993**, *11*, 25.

(55) Popovitcheva, O. B.; Trukhin, M. E.; Persiantseva, N. M.; Shonija, N. K. *Atmos. Environ.* **2001**, *35*, 1673.

(56) Busen, R.; Schumann, U. *Geophys. Res. Lett.* **1995**, *22*, 1357.

(57) Sorokin, A.; Arnold, F. *Atmos. Environ.* **2004**, *38*, 2611.

(58) Hagen, D. E.; Trueblood, M. B.; Whitefield, P. D. *Part. Sci. Technol.* **1992**, *10*, 53.